Biosafety and Health 6 (2024) 270–278

Contents lists available at ScienceDirect

Biosafety and Health

journal homepage: www.elsevier.com/locate/bsheal

Original Research

Drupacine as a potent SARS-CoV-2 replication inhibitor *in vitro*

Chen Yang [a], Yanying Yu [a], Qi Peng [b], Jingwei Song [a], Bo Sun [a], Yi Shi [b,1], Qiang Ding [a,c,1,*]

[a] School of Basic Medical Sciences, Tsinghua University, Beijing 100084, China
[b] CAS Key Laboratory of Pathogenic Microbiology and Immunology, Institute of Microbiology, Chinese Academy of Sciences, Beijing 100101, China
[c] SXMU-Tsinghua Collaborative Innovation Center for Frontier Medicine, Shanxi Medical University, Taiyuan 030001, China

ARTICLE INFO

Article history:
Received 13 July 2024
Revised 26 August 2024
Accepted 2 September 2024
Available online 3 September 2024

Keywords:
Severe acute respiratory syndrome coronavirus 2 (SARS-CoV-2)
High-content screening
Antiviral drug
Drupacine

ABSTRACT

Despite the availability of vaccines and antiviral treatments, the continued emergence of severe acute respiratory syndrome coronavirus 2 (SARS-CoV-2) variants and breakthrough infections underscores the need for new, potent antiviral therapies. In a previous study, we established a transcription and replication-competent SARS-CoV-2 virus-like particle (trVLP) system that recapitulates the complete viral life cycle. In this study, we combined high-content screening (HCS) with the SARS-CoV-2 trVLP cell culture system, providing a powerful phenotype-oriented approach to assess the antiviral potential of compounds on a large scale. We screened a library of 3,200 natural compounds and identified drupacine as a potential candidate against SARS-CoV-2 infection. Furthermore, we utilized a SARS-CoV-2 replicon system to demonstrate that drupacine could inhibit viral genome transcription and replication. However, *in vitro,* enzymatic assays revealed that the inhibition could not be attributed to conventional antiviral targets, such as the viral non-structural proteins nsp5 (MPro) or nsp12 (RdRp). In conclusion, our findings position drupacine as a promising antiviral candidate against SARS-CoV-2, providing a novel scaffold for developing anti-coronavirus disease 2019 therapeutics. Further investigation is required to pinpoint its precise target and mechanism of action.

1. Introduction

Severe acute respiratory syndrome coronavirus 2 (SARS-CoV-2) is the causative agent of the global pandemic, coronavirus disease 2019 (COVID-19) [1]. Since its emergence in late 2019, SARS-CoV-2 has inflicted substantial morbidity and mortality worldwide, severely impacting global health, economies, and societies [2]. The rapid transmission, coupled with the severity of symptoms ranging from mild respiratory distress to severe acute respiratory syndrome and death [3], underscores the urgent need for effective therapeutic interventions. Although some antiviral treatments are currently available, their effectiveness can be limited by resistance and variant-specific responses [4–11], highlighting the need for new antiviral agents that are broadly effective against diverse strains of SARS-CoV-2.

Repurposing approved drugs, target-based screening, and phenotypic screening are standard methods for drug discovery against new pathogens. Repurposing existing approved drugs is faster than *de novo* discovery due to available clinical data on safety and pharmacokinetics [12]. For instance, remdesivir and molnupiravir, initially developed for Ebola virus (EBOV) and Venezuelan equine encephalitis virus (VEEV), respectively, were repurposed for SARS-CoV-2 during the pandemic [13–15]. However, repurposed drugs may have suboptimal potency or undesirable adverse effects when used for new indications [16]. Target-based screening involves identifying and targeting specific viral proteins or host factors essential for the viral life cycle, such as the viral RNA-dependent RNA polymerase (RdRp) [17], main protease (MPro) [18–22], papain-like protease (PLpro) [23–27], and PIKfyve [28,29]. This method has also been the focus of computer-aided drug discovery for decades [30]. However, the transition of molecular inhibitors to effective cellular-level treatments is challenging. Many compounds fail to progress due to cytotoxicity and pharmacodynamic issues [16], resulting in a significant attrition rate. Moreover, the viral-host interactome's complexity and the identified targets' druggability pose significant challenges, necessitating extensive validation before advancing to antiviral development.

Phenotypic screening is a robust, untargeted approach that evaluates potential antivirals' impact on virus replication, cytopathic effects, virus yield, and plaque formation in infected cells [16,31]. This method benefits from not requiring prior knowledge of viral targets, thereby facilitating the discovery of novel antiviral agents that other screening techniques may overlook. However, conducting phenotypic screening for SARS-CoV-2 poses significant challenges due to the need

* Corresponding author: School of Basic Medical Sciences, Tsinghua University, Beijing 100084, China.
E-mail address: qding@tsinghua.edu.cn (Q. Ding).

[1] Given their roles as Editorial Board Member and Guest Editor, Yi Shi and Qiang Ding had no involvement in the peer-review of this article and had no access to information regarding its peer-review. Full responsibility for the editorial process for this article was delegated to Editor Yong Zhang.

https://doi.org/10.1016/j.bsheal.2024.09.001
2590-0536/

HIGHLIGHTS

Scientific question

The continued emergence of severe acute respiratory syndrome coronavirus 2 (SARS-CoV-2) variants and the limitations of current antiviral treatments underscore the need for novel and potent antiviral therapies. We aim to discover novel antivirals against SARS-CoV-2 infection.

Evidence before this study

Previous research has established a transcription and replication-competent SARS-CoV-2 virus-like particle (trVLP) cell culture system, which could recapitulate the entire viral life cycle in a Biosafety Level 2 (BSL-2) laboratory and enable high-throughput screening of antiviral compounds.

New findings

High-content screening (HCS) of 3,200 natural compounds using the trVLP system identified drupacine as an effective inhibitor of SARS-CoV-2 infection *in vitro*. A SARS-CoV-2 replicon system further confirmed that drupacine inhibits viral genome transcription and replication.

Significance of the study

The integration of the trVLP system with HCS facilitates large-scale, phenotypic compound screening against SARS-CoV-2 infection. The identification and exploration of druapcine as a potential SARS-CoV-2 inhibitor offer valuable insights into the development of antiviral therapies against the coronavirus disease 2019 (COVID-19).

for Biosafety Level 3 (BSL-3) laboratories. To address this, we developed a viral nucleocapsid (N) -based genetic complementation system to produce biologically contained, transcription and replication-competent SARS-CoV-2 virus-like particles (trVLPs) lacking *N* gene (SARS-CoV-2 ΔN trVLP). The absence of the viral N protein can be genetically complemented *in trans* by ectopic expression in packaging cells, allowing the production of SARS-CoV-2 ΔN trVLP. These SARS-CoV-2 ΔN trVLP can propagate and complete the entire viral life cycle in the packaging cells [32]. Additionally, a reporter gene can be inserted into the viral genome to monitor virus replication, thereby simplifying the monitoring of viral infection. This adjustment enables the rapid assessment of potential antivirals under BSL-2 conditions, significantly enhancing the feasibility of large-scale compound screening.

In this study, we opted to screen a library of natural compounds to discover novel antiviral lead compounds. The compound drupacine demonstrated the best efficacy among several identified potential antiviral agents. Further mechanistic studies using the SARS-CoV-2 replicon system revealed that drupacine inhibited viral replication, but interestingly, it did not target the common antiviral sites nsp5 or nsp12. Our study provides a new scaffold for developing anti-COVID-19 drugs and indicates the necessity for further research to fully elucidate its target and mechanism of action.

2. Materials and methods

2.1. Cell culture

HEK293T, Caco2-N, and S10-3-N cells were maintained in Dulbecco's modified Eagle medium (DMEM) (Gibco, NY, USA) supplemented with 10 % (vol / vol) fetal bovine serum (FBS) and 50 IU / mL penicillin/streptomycin in a humidified 5 % (vol / vol) CO_2 incubator at 37 ℃. Cells were routinely tested by polymerase chain reaction (PCR) and no detectable mycoplasma contamination was found.

2.2. SARS-CoV-2 trVLP generation and amplification

The detailed protocol of production and amplification of SARS-CoV-2 trVLP had been previously described [32,33]. Briefly, SARS-CoV-2 trVLP genome RNA and *N* gene mRNA were *in vitro* transcribed by the mMESSAGE mMACHINE T7 Transcription Kit (AM1344, ThermoFisher Scientific) according to the manufacturer's instruction and then transfected into Caco2-N cells by electroporation. The Passage 0 (P0) virus was collected and used for amplification three days post-electroporation.

2.3. Chemicals and reagents

The BioBioPha (BBP) Natural Product Library, housed at the Center of Pharmaceutical Technology, Tsinghua University (Beijing, China), was utilized for high-throughput screening (HTS) and dose–response studies. The collection was provided in 384-well plates, with each compound dissolved to 5 mg / mL in dimethyl sulfoxide (DMSO) and stored at − 20 ˚C until use. Drupacine (BBP03468) was acquired from BioBioPha. Remdesivir was purchased from MedChemExpress (HY-104077). DMSO was purchased from Sigma (D2650-100ML).

2.4. High-content screening assay

One day before infection, Caco2-N cells were seeded in clear 96-well plates (167008, ThermoFisher Scientific) at a density of 30,000 cells per well. The 5 mg / mL drug stocks were thawed at 25 ˚C for 1 h before use. Using the Echo550 Liquid Handler (Labcyte), 50 nL of each compound was transferred into empty 96-well round-bottom plates (163320, ThermoFisher Scientific). Positive control (10 mmol / L Remdesivir in DMSO) and negative control (DMSO) were processed similarly. Next, 100 μL of a SARS-CoV-2 trVLP dilution in DMEM (containing 10 % FBS, 50 IU / mL penicillin / streptomycin) was added to achieve a final drug concentration of 2.5 μg / mL (0.05 % DMSO, vol / vol) and a multiplicity of infection (MOI) of 0.05. The drug-virus mixture replaced the culture medium of Caco2-N cells. At 24 h post-infection, the cells were fixed with 4 % paraformaldehyde (PFA) supplied by Leagene at room temperature for 15 min and stained with 1 μg / mL of 4',6-diamidino-2-phenylindole (DAPI), which was dissolved in phosphate buffered saline (PBS), for a duration of 2 h. The samples were analyzed using Opera Phenix high-content screening system (PerkinElmer) and Harmony software (PerkinElmer) to determine the total and green fluorescent protein (GFP)-positive cell numbers across five fields from each well. The quality of each plate was assessed by calculating the Z' factor by the formula $Z' = 1 - 3 \times$ [standard deviation (SD) of positive control + SD of negative control] / |mean of positive control – mean of negative control| [34]. Finally, each compound's infection rate and cell number were normalized to those of the negative control on the same plate for summarization.

2.5. Half maximal (50 %) inhibitory concentration (IC_{50}) determination

Caco2-N cells were infected by SARS-CoV-2 trVLP at an MOI = 0.05. Colelomycerone A, Parvifolixanthone B, or drupacine were added at varying concentrations ranging from 20 μmol / L to 0.256 nmol / L. After incubation, the cells were harvested and analyzed by flow cytometry using BD LSRFortessa SORP. Data were processed with FlowJo software (version 10) to determine the percentage of GFP-positive cells, serving as a proxy of viral infection. The IC_{50} values were calculated by fitting the data to the model “log

(inhibitor) vs. normalized response − variable slope" using Prism GraphPad 8.4.3 (GraphPad Software).

2.6. Half maximal (50 %) cytotoxic concentration (CC_{50}) determination

Caco2-N cells were seeded in 96-well plates at a density of 5,000 cells per well and cultured overnight at 37 ℃. The following day, cells were incubated with serially diluted compounds for 72 h. Cell viability was assessed using the CellTiter-Glo® Reagent Kit (G7571, Promega) according to the manufacturer's instructions. Luminescence was measured in opaque-walled 96-well plates using a Promega luminometer. The CC_{50} values were calculated by fitting the data to the model "log (inhibitor) vs. normalized response − variable slope" using Prism GraphPad 8.4.3 (GraphPad Software). DMSO-only samples were used as 100 % cell viability controls.

2.7. Construction, in vitro transcription and transfection of SARS-CoV-2 sGluc replicon

For the construction of SARS-CoV-2 secreted Gaussia luciferase (sGluc) replicon complementary deoxyribonucleic acid (cDNA), the fragments of the SARS-CoV-2 sGluc replicon cDNA templates were amplified by PCR using high fidelity PrimeSTAR MAX DNA Polymerase (R045A, Takara). These fragments were assembled into the pGFCS vector in the VL6-48B yeast strain via transformation-associated recombination (TAR) as previously described [35]. *In vitro* transcription assay was performed to obtain the replicon ribonucleic acid (RNA). In brief, the plasmid bearing the SARS-CoV-2 sGluc replicon cDNA was linearized using AgeI-HF restriction endonuclease (R3552L, NEB). The linearized plasmid served as the template for *in vitro* transcription using the mMESSAGE mMACHINE T7 Transcription Kit (AM1344, ThermoFisher Scientific). According to the manufacturer's instructions, the transcribed viral replicon RNA was transfected into cells using the TransIT-mRNA transfection reagent (MIR2250, Mirus Bio). The supernatant was harvested at indicated time points and stored at −20 ℃. The remaining culture medium was refreshed to maintain cell viability.

2.8. FRET-based assay for nsp5 protease activity

The detailed protocols for SARS-CoV-2 nsp5 expression, purification, enzymatic activity, and inhibition assays have been previously described [19]. The nsp5 protease activity was measured using a continuous kinetic assay monitored with an EnVision multimode plate reader (PerkinElmer). The assay utilized excitation and emission wavelengths of 320 nm and 405 nm, respectively. For the inhibition assay, the reaction mixture contained 40 μg / mL of nsp5, 20 μmol / L of the substrate (MCA-AVLQ↓SGFR-K (Dnp) K, G.L. Biochem), and varying concentrations of inhibitors ranging from 25 μmol / L to 0.025 nmol / L. The signal at 405 nm, indicating nsp5 activity, was recorded continuously to assess the inhibitory effects of the tested compounds.

2.9. Primer extension assay for RdRp activity

Detailed protocols for SARS-CoV-2 nsp7, nsp8, and nsp12 expression, purification, and assays for RdRp complex activity and inhibition have been previously established [36]. Briefly, a 40-nucleotide template RNA (5′- CUA UCC CCA UGU GAU UUU AAU AGC UUC UUA GGA GAA UGA C-3′, Takara) representing the 3′ terminus of the SARS-CoV-2 genome was hybridized to a 5′ fluorescein-labeled complementary primer (5′FAM-GUC AUU CUC CUA AGA AGC UA-3′, Takara). The annealed RNA complex was incubated with the nsp12, nsp7, and nsp8 proteins in a reaction buffer consisting of 0.5 mmol / L of NTP, 10 mmol / L Tris-HCl (pH 8.0), 10 mmol / L KCl, 1 mmol / L beta-mercaptoethanol, and 2 mmol / L $MgCl_2$, at 30 ℃ for 30 min. Following incubation, the reaction products were denatured and resolved by polyacrylamide gel electrophoresis (PAGE) to analyze the activity and inhibition of the RdRp complex.

2.10. Western blot

Cells were washed with phosphate-buffered saline (PBS) and lysed in 1 × sodium dodecyl sulfate (SDS) loading buffer consisting of 50 mM Tris-HCl (pH 6.8), 10 % (v / v) glycerol, 2 % (w / v) sodium dodecyl sulfate (SDS), 1 % (w / v) dithiothreitol (DTT), 0.1 % bromophenol blue (BPB). Then, the whole-cell lysates were heated for 10 min at 95 °C before being separated on a 4 %–12 % SDS polyacrylamide gel and transferred to a polyvinylidene fluoride (PVDF) membrane (Millipore) after blocking with 5 % nonfat milk in 1 × PBS containing 0.1 % (v / v) Tween 20, incubation with the primary antibody anti-β-actin (Abcepta), or anti-Flag (Sigma) in 5 % nonfat milk in 1 × PBS containing 0.1 % Tween 20 for 2 h. The secondary horseradish peroxidase (HRP)-coupled goat anti-mouse IgG antibody (Abclonal) was applied at 1:10,000 in PBS for one hour at room temperature. For detection, the enhanced chemiluminescence (ECL) substrate (BE6706-250, Easybio) was used according to the manufacturer's protocol. Subsequent washes were performed and membranes were visualized using the Luminescent image analyzer (G.E.).

2.11. Statistical analysis

Unless otherwise mentioned, results are represented as means ± SD determined using GraphPad Prism 8 (GraphPad Software, La Jolla, CA). Dose-response curves were analyzed and fitted with the model' log (inhibitor) vs. normalized response – variable slope' in GraphPad Prism 8. One-way analysis of variance (ANOVA) with Dunnett's honestly significant difference (HSD) test was used to test for the statistical significance of the differences between the control group and other groups. *P* values of less than 0.05 were considered statistically significant.

3. Results

3.1. High-content screening using SARS-CoV-2 trVLP identifies three promising antivirals

To efficiently evaluate candidate antivirals in the BSL-2 platform, we utilized a viral N-based trans-complementation cell culture system designed to model authentic SARS-CoV-2 infection, termed SARS-CoV-2 trVLP [32]. In this system, the *N* gene in the SARS-CoV-2 genome is replaced with a GFP reporter gene within the trVLP genome (SARS-CoV-2 ΔN / GFP trVLP), enabling direct visualization of viral infection under fluorescent microscopy. Viral replication is biologically contained in cells with the N protein, ensuring biosafety (Fig. 1A). High-content screening (HCS), which involves automated image acquisition and analysis to assess multiple properties of individual cells, has emerged as a powerful tool for large-scale drug screening against emerging pathogens [37]. Caco2-N cells transduced with the SARS-CoV-2 *N* gene via lentivirus were infected with SARS-CoV-2 ΔN / GFP trVLP in the presence of remdesivir or DMSO and fixed 24 h post-infection for HCS imaging analysis to validate whether HCS can be applied in the trVLP-based platform. GFP positivity served as a proxy for virus infection. We observed a dramatic difference in GFP positivity between the DMSO and remdesivir groups in each field (Fig. 1B). In conclusion, these results demonstrate that HCS is a robust and straightforward assay for SARS-CoV-2 trVLP-based antiviral screening. This approach provides an efficient means to identify potential antiviral candidates under BSL-2 laboratory conditions.

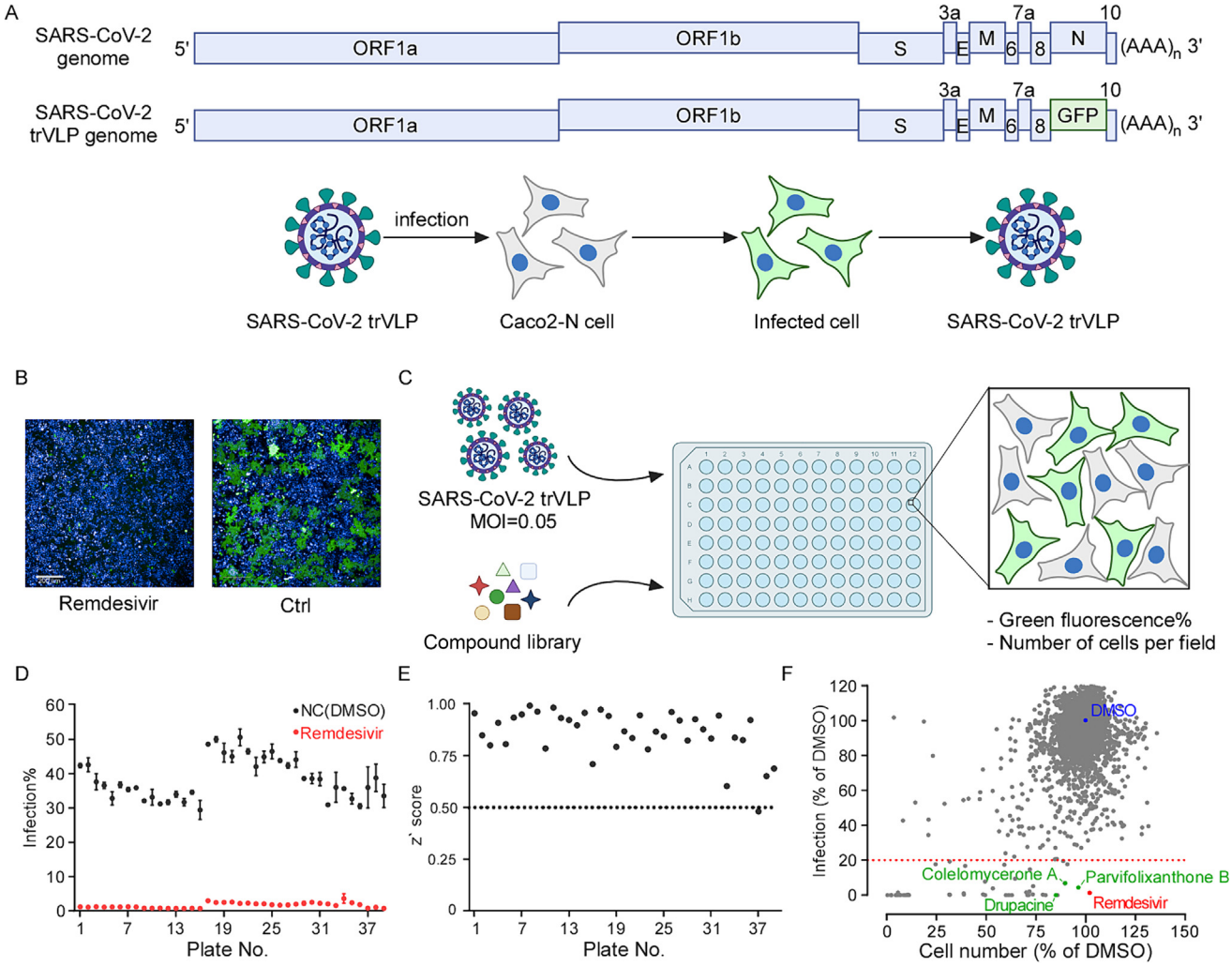

Fig. 1. High-content screening of antivirals using SARS-CoV-2 trVLP. A) Schematic diagram of the SARS-CoV-2 trVLP genome and infection. The *N* gene is replaced with a GFP reporter gene to visualize infection in Caco2-N cells, a cell line stably expressing the N protein, ensuring biosafety at a BSL-2 level. B) HCS images of Caco2-N cells infected with SARS-CoV-2 trVLP, treated with either 5 μmol / L Remdesivir or 0.5 % DMSO (solvent control). C) Workflow of HCS for antivirals against SARS-CoV-2. Briefly, compounds at 2.5 μg / mL together with SARS-CoV-2 trVLP (MOI = 0.05) were added to 96-well plates seeded with Caco2-N cells. At 24 h post-infection, the cells were fixed, stained with DAPI, and subject to HCS imaging to determine the GFP positive rate and cell count, representing viral infection and cytotoxicity, respectively. D) Distribution of infection rates of solvent control groups (black, n = 3 biological replicates per plate) and remdesivir-treated groups (red, n = 3 biological replicates per plate) from each 96-well plate used in the screening. E) Scatter plot of Z' factors calculated for quality control of the screening plates, with those scoring values above 0.5 considered qualified for further analysis. F) Screening result of 3,200 compounds from the BioBioPha (BBP) Natural Product Library natural compound library. The red dotted line represents the threshold (normalized infection < 20 %) for positive hit compounds. DMSO (blue) and remdesivir (red) were used as controls in the screening. Each dot represents a single compound, with green dots indicating promising candidates that exhibited potent antiviral activity without dramatic cytotoxicity. Abbreviations: SARS-CoV-2, severe acute respiratory syndrome coronavirus 2; trVLP, transcription and replication-competent virus-like particle; ORF, opening reading frame; GFP, green fluorescent protein; BSL, biosafety level; HCS, high-content screening; DMSO, dimethyl sulfoxide; Ctrl, control; DAPI, 4',6-diamidino-2-phenylindole; MOI, multiplicity of infection.

Biologically active compounds extracted and purified from traditional Chinese herbal plants have been regarded as a promising resource for discovering new antivirals. Some molecules, such as cepharanthine [38–40] and lycorine [32,41], have been identified as potential SARS-CoV-2 inhibitors. Thus, the BBP Natural Product Library, containing 3,200 natural compounds, was selected for screening. All compounds were tested at a final concentration of 2.5 μg / mL, which were added into the cell culture along with SARS-CoV-2 trVLP infection. Twenty-four hours post-infection, HCS imaging analysis was conducted to quantify the number of cells (indicated by the number of nuclei) and GFP positivity rate of each well (Fig. 1C). Remdesivir and DMSO were positive and negative controls on each plate, respectively. The GFP positivity rate in the DMSO group on each plate ranged from 30 % to 50 %, while in the remdesivir group, it was lower than 2 % (Fig. 1D). Furthermore, Z' scores were calculated as quality control for each plate, and plates with Z' scores greater than 0.5 were further analyzed (Fig. 1E).

Each sample's infection rate and cell number were normalized against the DMSO group on its respective plate to eliminate inter-plate variation. For each compound, antiviral activity was indicated by a decrease in the infection rate, while a decrease in cell number indicated cytotoxicity. The results showed that tens of hits met the criterion of a normalized infection rate lower than 20 % (the red line, Fig. 1F). However, most of these hits were excluded due to significant cytotoxicity, evidenced by a sharp decline in cell number. Ultimately, colemycerone A, parvifolixanthone B, and drupacine (marked in green in Fig. 1F) were selected for further assessment due to their outstanding antiviral performance and low cytotoxicity.

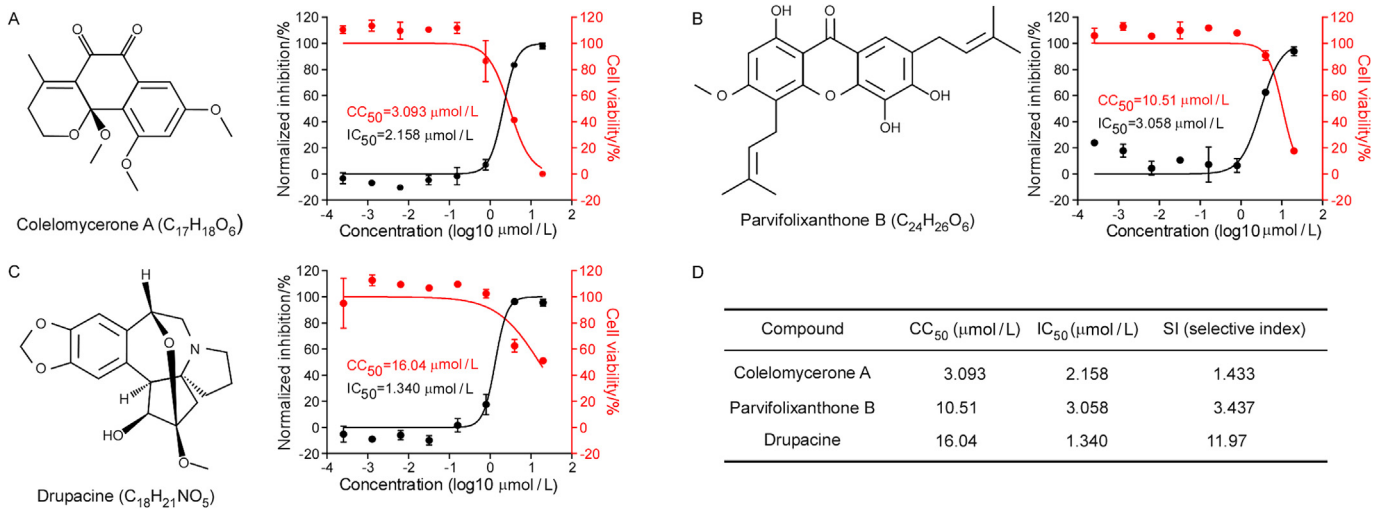

Compound	CC_{50} (μmol/L)	IC_{50} (μmol/L)	SI (selective index)
Colelomycerone A	3.093	2.158	1.433
Parvifolixanthone B	10.51	3.058	3.437
Drupacine	16.04	1.340	11.97

Fig. 2. Dose-response curves and cytotoxicity determination of antiviral candidates against SARS-CoV-2 trVLP infection. A) - C) Molecular structures and dose–response curves of selected hit compounds: colemycerone A, parvifolixanthone B and drupacine. IC_{50} and CC_{50} values were calculated using Prism software and are representative of one of three independent experiments. D) Summary of dose–response determinations. The table lists CC_{50}, IC_{50}, and selective index (CC_{50} / IC_{50}) for each compound. Abbreviations: SARS-CoV-2, severe acute respiratory syndrome coronavirus 2; trVLP, transcription and replication-competent virus-like particle; IC_{50}, half maximal (50 %) inhibitory concentration; CC_{50}, half maximal (50 %) cytotoxic concentration.

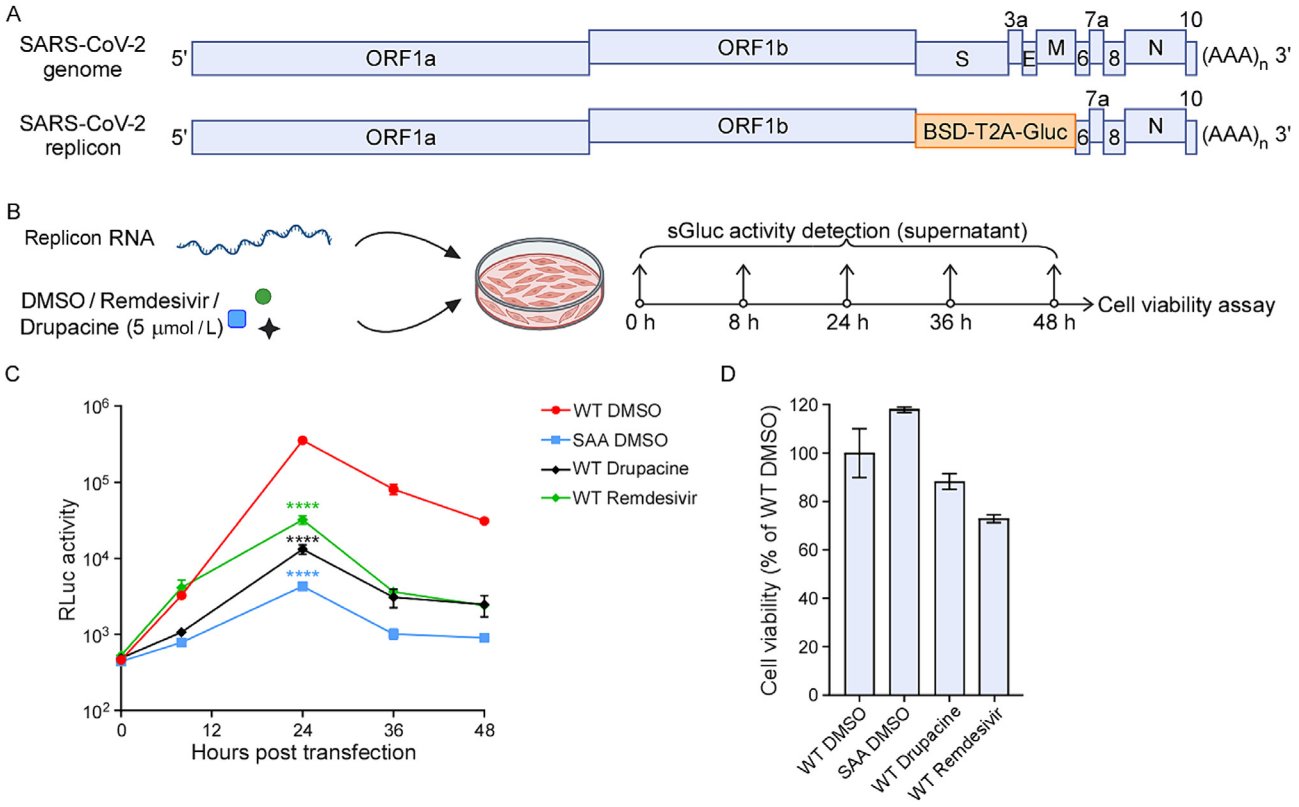

Fig. 3. Drupacine inhibits SARS-CoV-2 replicon activity. A) Scheme of the SARS-CoV-2 replicon. Compared to the complete SARS-CoV-2 viral genome, the S, ORF3a, E and M genes are replaced by the BSD-T2A-Gluc reporter gene, allowing transcription and replication to be monitored via sGluc activity in the cell culture supernatant. B) Overview of the experimental setup. S10-3-N cells were transfected with the WT replicon RNA and treated with either 5 μmol / L remdesivir, drupacine, or DMSO. SAA replicon RNA-transfected cells were treated with DMSO to serve as a non-replicating control. The sGluc activity of each group was monitored at 8, 24, 36, 48 h post-transfection. Additionally, cell viability for each group was determined at 48 h post-transfection. C) Kinetics of sGluc activity across the four groups: WT-DMSO (red), SAA-DMSO (blue), WT-drupacine (black), and WT-remdesivir (green). The sGluc activity indicates replicon transcription and replication. Significance assessed by one-way ANOVA; the asterisks represent significant differences: ****, $P<0.0001$. D) Cell viability of each group determined at 48 h post-transfection. The original cell viability data were normalized to that of the WT-DMSO group. Error bars represent the standard deviation (SD) for three replicates. Abbreviations: SARS-CoV-2, severe acute respiratory syndrome coronavirus 2; trVLP, transcription and replication-competent virus-like particle; BSD, blasticidin; Gluc, Gaussia luciferase; sGluc, secreted Gaussia luciferase; WT, wild-type; DMSO, dimethyl sulfoxide; SAA, SARS-CoV-2 nsp12 protein carrying SDD 759–761 SAA mutations; RNA, ribonucleic acid; ANOVA, analysis of variance; ORF, opening reading frame.

3.2. Dose-response analysis and cytotoxicity assessment of antiviral candidates

As the compounds were only tested at 2.5 μg / mL in the screening, we further evaluated the antiviral activity of these candidates at various concentrations. Caco2-N cells were infected with SARS-CoV-2 trVLP at an MOI of 0.05 in the presence of varying doses of compounds. The cells were harvested to determine GFP positive rate by flow cytometry 24 h post-infection. Meanwhile, cytotoxicity caused by the compound treatment was measured. For colemycerone A, the CC_{50} was 3.093 μmol / L, the IC_{50} was 2.158 μmol / L, and the selective index (SI) was 1.433 (Fig. 2A). For parvifolixanthone B, the CC_{50} was 10.51 μmol / L, the IC_{50} was 3.058 μmol / L, and the SI was 3.437 (Fig. 2B). Among these candidates, drupacine exhibited the highest CC_{50} (16.04 μmol / L) and the lowest IC_{50} (1.340 μmol / L) (Fig. 2C), resulting in the most favorable SI (Fig. 2D). Drupacine's high CC_{50} and low IC_{50} suggest its antiviral effect with minimal cytotoxicity, making it a promising candidate for further study. Its high selective index indicates a potential therapeutic window, reducing the likelihood of off-target effects and toxicity. This compound's potential mechanism of action and specific antiviral targets warrant further investigation to fully understand its efficacy and optimize its use as a therapeutic agent against SARS-CoV-2.

3.3. Drupacine inhibits SARS-CoV-2 replicon replication

Drupacine has been previously reported as a nematode pesticide, functioning as a protease inhibitor specific to nematodes [42]. We hypothesized that drupacine might similarly inhibit nsp5, the main protease (MPro) of SARS-CoV-2, thus reducing viral genome replication. We used a SARS-CoV-2 replicon system to test this hypothesis and mimic the transcription-replication step in the viral life cycle. In this system, the genes encoding structural proteins S, E, and M, and ORF3a are replaced by the sGluc reporter gene, allowing measurement of viral transcription and replication through supernatant luciferase activity (Fig. 3A). S10-3-N cells, transduced with the SARS-CoV-2 *N* gene via lentivirus, were transfected with wild-type (WT) replicon RNA and treated with 5 μmol / L remdesivir, drupacine, or an equal amount of DMSO. As a non-replication control, cells were also transfected with SAA replicon RNA, which carries an enzymatically dead mutation (nsp12 protein: SDD 759–761 SAA), and treated with DMSO [43,44]. The sGluc signal of each group was monitored at various time points (8, 24, 36, and 48 h post-transfection) (Fig. 3B). As expected, the sGluc activity in the WT group (red, Fig. 3C) exhibited a sharp increase and peaked at 24 h post-transfection, while the SAA mutant group (blue, Fig. 3C) showed a limited increase. As expected, remdesivir effectively inhibited SARS-CoV-2 replication, as evidenced by an approximately 10-fold reduction in sGluc signal compared with DMSO-treated WT replicon cells (green, Fig. 3C). Notably, drupacine treatment also effectively inhibited SARS-CoV-2 replication (black, Fig. 3C), leading to a significant reduction (-100 fold) in sGluc signal compared with DMSO-treated WT replicon cells at 24 h post-transfection. A cell viability assay confirmed that the decline in sGluc activity was not due to cytotoxicity (Fig. 3D). Our results indicate that drupacine inhibits SARS-CoV-2 infection by reducing viral genome replication.

3.4. Drupacine did not inhibit SARS-CoV-2 MPro or RdRp in vitro

Drupacine may inhibit replicon activity by targeting viral proteins required for translation and replication. We investigated this and tested whether drupacine directly inhibited essential viral non-structural proteins, specifically nsp5 (MPro) and nsp12 (RdRp).

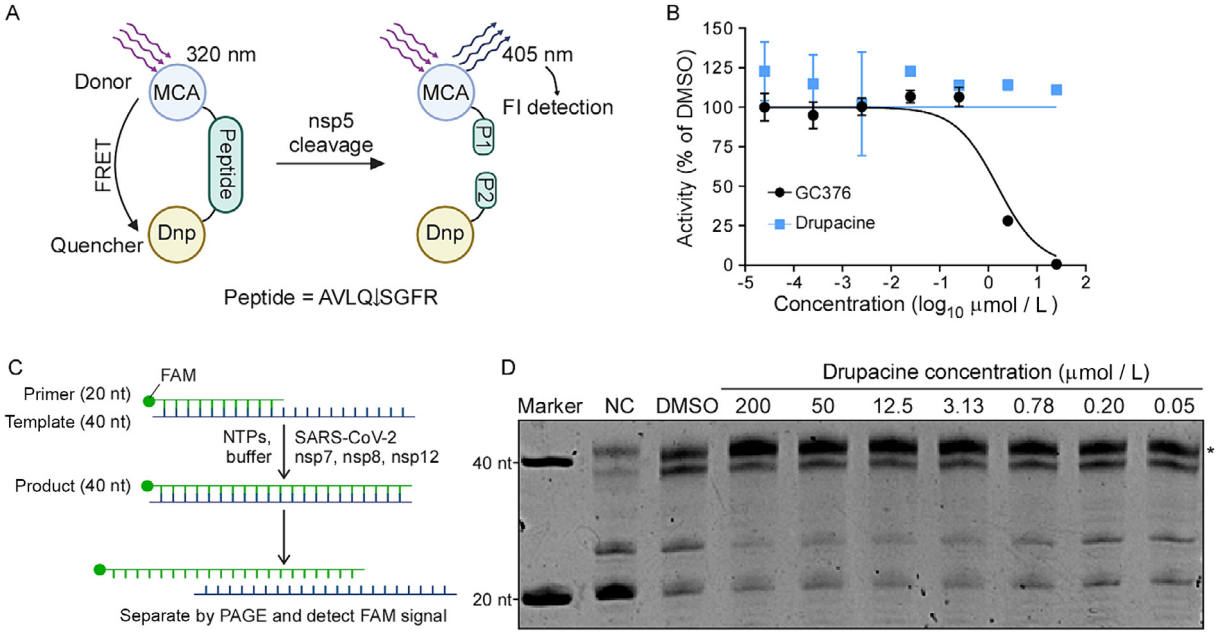

Fig. 4. Drupacine did not directly inhibit viral nsp5 or RdRp activity. A) Schematic of the FRET-based assay for measuring SARS-CoV-2 nsp5 protease activity. The substrate consists of MCA, a linker peptide (AVLQ|SGFR, with the cleavage site for nsp5 marked), and Dnp. Cleavage of the peptide produces fluorescence at 405 nm. B) Dose-response curve of nsp5 activity in the presence of GC376 (positive control) and drupacine. The nsp5 enzymatic activity data were normalized to the DMSO-treated group. Error bars represent the SD of three replicates. C) Workflow of the primer extension assay to measure the activity of the SARS-CoV-2 nsp7-nsp8-nsp12 RdRp complex. The active RdRp complex is expected to elongate the 20-nt primer to 40-nt product. D) Gel image of the primer extension assay, representative of one of two independent experiments. The band of the expected extension product at 40-nt is marked (*). NC (negative control) indicates that no extra reagent was added to the reaction system. DMSO represents the 10 % DMSO solvent control. Drupacine concentration ranged from 200 μmol / L to 0.05 μmol / L (4 × per gradient) in the reaction, with the same amount of DMSO (10 %, vol / vol). Abbreviations: FRET, fluorescence resonance energy transfer; MCA, 7-methoxycoumarin-4-acetyl; Dnp, 2,4-dinitrophenyl; DMSO, dimethyl sulfoxide; SD, standard deviation; RdRp, RNA-dependent RNA polymerase; nt, nucleotide; PAGE, polyacrylamide gel electrophoresis; FI, fluorescence intensity.

We employed fluorescence resonance energy transfer (FRET) to test drupacine's inhibition of nsp5 activity [19]. The donor (MCA) is linked to the quencher (Dnp) via the peptide in the FRET assay. When the peptide is intact, the photon emitted by the donor molecule is quenched by the adjacent quencher molecule. Enzymatic cleavage of the peptide by nsp5 separates the donor from the quencher, resulting in detectable fluorescence at 405 nm. Thus, the protease activity of nsp5 is quantified by the increasing rate of relative fluorescence intensity unit (RFU) with time (Fig. 4A). GC376, a known SARS-CoV-2 nsp5 inhibitor [20,45,46], served as a positive control. The recombinant SARS-CoV-2 nsp5 protein was incubated with the substrate (MCA-AVLQ|SGFR-Dnp) and various concentrations of GC376 or drupacine in the reaction buffer. We monitored the fluorescence changes over time and assessed the nsp5 activity of each group. The result showed that GC376 inhibited nsp5 activity in a dose-dependent manner, while drupacine did not inhibit nsp5 substrate cleavage within the tested range (Fig. 4B), indicating that drupacine does not directly inhibit SARS-CoV-2 nsp5 activity *in vitro*.

Nsp12 is the RNA-dependent RNA polymerase of SARS-CoV-2, but it requires the cofactors nsp7 and nsp8 to form the minimal core component capable of viral RNA synthesis [36,47]. To investigate whether drupacine directly inhibits the nsp12-nsp7-nsp8 complex, we conducted a primer extension assay using purified nsp12, nsp7, and nsp8 proteins, a FAM-labeled 20-nt primer RNA, and a 40-nt template RNA [36] (Fig. 4C). The active nsp12-nsp7-nsp8 complex successfully synthesized the 40-nt product in the control panel with DMSO. If a compound inhibits RdRp activity, like favipiravir, the 40-nt product would sharply decrease [48]. However, in the presence of various concentrations of drupacine (ranging from 200 μmol / L to 0.05 μmol / L), the gel image showed negligible changes in the quantity of the 40-nt extension product compared to the DMSO control. These results indicated that the amount of extension product was minimally affected by drupacine (Fig. 4D), demonstrating that drupacine does not directly inhibit the RdRp complex activity *in vitro*.

In summary, although drupacine inhibits SARS-CoV-2 replicon activity and is an inhibitor of the viral replication cycle, it does not directly inhibit viral MPro and RdRp *in vitro*. These findings suggest that drupacine may target other viral proteins or critical host factors involved in viral replication.

4. Discussion

Our study employed a SARS-CoV-2 trVLP system to screen potential antivirals from a natural compound library (Fig. 1A). The combination of trVLP and HCS provided a robust and efficient phenotype-oriented method for identifying anti-SARS-CoV-2 compounds, suitable for large-scale screenings (Fig. 1B and 1E). We identified three promising antivirals: colemycerone A, parvifolixanthone B, and drupacine (Fig. 1F). Further evaluation demonstrated that drupacine had a favorable SI, indicating its potential as a therapeutic agent (Fig. 2). Additionally, our replicon inhibition assay suggested that Drupacine acts as a transcription-replication inhibitor for SARS-CoV-2 (Fig. 3).

To elucidate the antiviral mechanism of drupacine, we tested its effect on critical non-structure proteins known to be therapeutic targets, such as nsp5 (MPro) and RdRp complex (nsp7 / 8 / 12). However, drupacine did not directly inhibit their protease or polymerase activities (Fig. 4A-4D). Findings shown above suggest that drupacine or its metabolites may play a critical role in antiviral activity, akin to remdesivir and its active metabolite remdesivir triphosphate [49]. Another possible explanation is that drupacine targets other viral enzymes, such as the capping enzyme nsp9 [50] or the helicase nsp13 [51]. Clarifying drupacine's specific target could open avenues for combination therapies, where drupacine is paired with other antivirals that act on different targets or even different stages of the viral life cycle. Such strategies could enhance therapeutic efficacy, minimize side effects, and reduce the risk of the virus developing resistance [52–55]. Further research is needed to explore these possibilities and fully understand the antiviral mechanism of drupacine.

Drupacine itself is not well-studied, but homoharringtonine (HHT), a related cephalotaxine (CET)-type alkaloid, is known for its antiproliferative and antiviral properties [56,57]. HHT has shown efficacy against viruses such as vesicular stomatitis virus (VSV), Newcastle disease virus (NDV), herpes simplex virus type 1 (HSV-1), and porcine epidemic diarrhea virus (PEDV) [58]. HHT inhibits PEDV by reducing the eukaryotic initiation factor 4E (eIF4E) phosphorylation, which we hypothesized might apply to Drupacine as well [58]. Given the antiviral activities observed for drupacine and HHT, it would be prudent to extend investigations to more CET-type alkaloids to determine if this class uniformly possesses antiviral properties and whether the CET scaffold contributes fundamentally to these effects. Modifications and enhancements of the CET scaffold could be valuable for developing future broad-spectrum antiviral medications. Antiviral studies on HHT also suggest that we could not exclude the possibility that drupacine might target eIF4E or other essential host factors. Identifying whether drupacine targets specific viral proteins or host factors involved in viral replication would provide deeper insights into its mechanism of action and inform the design of combination therapies to enhance therapeutic efficacy and mitigate resistance development.

Despite these promising findings, our study has several limitations. Firstly, antiviral candidates were evaluated primarily at protein and cell levels. Further studies must assess their efficacy in more physiological systems, such as animal models. Additionally, while drupacine exhibited potent antiviral activity, its safety profile and potential off-target effects necessitate comprehensive investigation, including detailed pharmacokinetic and pharmacodynamic studies to ascertain its behavior in biological systems, its interaction with other pharmaceuticals, and any potential for adverse effects. All of them are essential steps before clinical application. Finally, although drupacine emerged as a leading candidate from our screening of 3,200 natural compounds, its IC_{50}, CC_{50}, and SI values indicate that it does not demonstrate a remarkable advantage over currently known antiviral drugs, such as camostat [59–61] and hydroxychloroquine [62–65], which have already been disqualified in subsequent animal and clinical trials. The failure underscores the ongoing challenge and complexity of discovering and developing the next effective antiviral drug.

In conclusion, our study demonstrated the utility of a phenotype-oriented HCS platform using SARS-CoV-2 trVLP for antiviral screening in a BSL-2 setting. We screened 3,200 natural compounds and identified drupacine as a novel inhibitor of SARS-CoV-2 replication. While further research is required to elucidate its antiviral mechanism and evaluate its therapeutic efficacy in animal models, our findings provide a promising candidate for further development against COVID-19.

Acknowledgements

We thank the staff of the Center of Pharmaceutical Technology, Tsinghua University for their valuable advice and assistance with the high-content screening. We are also grateful to Dr. Zhiyong Lou and Dr. Zihe Rao (Tsinghua University) for the expert guidance on the purification and activity assay of nsp5. This work was supported by the National Natural Science Foundation of China (82341084, 82241077, 82272302, and 32070153), National Key Research and Development Plan of China (2023YFC2305900 and 2021YFC2300200-04), Tsinghua University Dushi Program (20231080039), and SXMU-Tsinghua Collaborative Innovation Center for Frontier Medicine. The funders had no role in study design, data collection and analysis, publication decisions, or manuscript preparation.

Conflict of interest statement

The authors declare that there are no conflicts of interest.

Author contributions

Chen Yang: Writing – original draft, Visualization, Validation, Investigation, Formal analysis, Data curation. **Yanying Yu:** Methodology. **Qi Peng:** Investigation. **Jingwei Song:** Investigation. **Bo Sun:** Investigation. **Yi Shi:** Supervision. **Qiang Ding:** Writing – review & editing, Supervision, Resources, Project administration, Methodology, Investigation, Funding acquisition, Data curation, Conceptualization.

References

[1] P. Zhou, X.L. Yang, X.G. Wang, B. Hu, L. Zhang, W. Zhang, H. Si, Y. Zhu, B. Li, C.L. Huang, et al., A pneumonia outbreak associated with a new coronavirus of probable bat origin, Nature 579 (2020) 270–273, https://doi.org/10.1038/s41586-020-2012-7.

[2] E. Dong, H. Du, L. Gardner, An interactive web-based dashboard to track COVID-19 in real time, Lancet Infect. Dis. 20 (2020) 533–534, https://doi.org/10.1016/S1473-3099(20)30120-1.

[3] C. Huang, Y. Wang, X. Li, L. Ren, J. Zhao, Y. Hu, L. Zhang, G. Fan, J. Xu, X. Gu, et al., Clinical features of patients infected with 2019 novel coronavirus in Wuhan, China, The Lancet 395 (2020) 497–506, https://doi.org/10.1016/S0140-6736(20)30183-5.

[4] S. Gandhi, J. Klein, A.J. Robertson, M.A. Peña-Hernández, M.J. Lin, P. Roychoudhury, P. Lu, J. Fournier, D. Ferguson, S.A.K. Mohamed Bakhash, et al., De novo emergence of a remdesivir resistance mutation during treatment of persistent SARS-CoV-2 infection in an immunocompromised patient: a case report, Nat. Commun. 13 (2022) 1547, https://doi.org/10.1038/s41467-022-29104-y.

[5] A. Heyer, T. Günther, A. Robitaille, M. Lütgehetmann, M.M. Addo, D. Jarczak, S. Kluge, M. Aepfelbacher, J. Schulze Zur Wiesch, N. Fischer, A. Grundhoff, et al., Remdesivir-induced emergence of SARS-CoV2 variants in patients with prolonged infection, Cell Rep. Med. 3 (2022) 100735, https://doi.org/10.1016/j.xcrm.2022.100735.

[6] J.T. Lee, Q. Yang, A. Gribenko, B.S. Perrin, Y. Zhu, R. Cardin, P.A. Liberator, A.S. Anderson, L. Hao, Genetic surveillance of SARS-CoV-2 Mpro reveals high sequence and structural conservation prior to the introduction of protease inhibitor paxlovid, mBio 13 (2022) e00869-22. https://doi.org/10.1128/mbio.00869-22.

[7] S. Iketani, H. Mohri, B. Culbertson, S.J. Hong, Y. Duan, M.I. Luck, M.K. Annavajhala, Y. Guo, Z. Sheng, A.-C. Uhlemann, et al., Multiple pathways for SARS-CoV-2 resistance to nirmatrelvir, Nature 613 (2023) 558–564, https://doi.org/10.1038/s41586-022-05514-2.

[8] E. Birnie, J.J. Biemond, B. Appelman, G.J. de Bree, M. Jonges, M.R.A. Welkers, W. J. Wiersinga, Development of resistance-associated mutations after sotrovimab administration in high-risk individuals infected with the SARS-CoV-2 omicron variant, JAMA 328 (2022) 1104–1107, https://doi.org/10.1001/jama.2022.13854.

[9] J.D. Ip, A.W.H. Chu, W.M. Chan, R.C.Y. Leung, S.M.U. Abdullah, Y. Sun, K. W. To, Global prevalence of SARS-CoV-2 3CL protease mutations associated with nirmatrelvir or ensitrelvir resistance, eBioMedicine 91 (2023) 104559, https://doi.org/10.1016/j.ebiom.2023.104559.

[10] Y. Hu, E.M. Lewandowski, H. Tan, X. Zhang, R.T. Morgan, X. Zhang, L.M.C. Jacobs, S.G. Butler, M.V. Gongora, J. Choy, et al., Naturally occurring mutations of SARS-CoV-2 main protease confer drug resistance to nirmatrelvir, ACS Cent. Sci. 9 (2023) 1658–1669, https://doi.org/10.1021/acscentsci.3c00538.

[11] M. Ibrahim, X. Sun, V.M. de Oliveira, R. Liu, J. Clayton, H. El Kilani, J. Shen, R. Hilgenfeld, Why is the omicron main protease of SARS-CoV-2 less stable than its wild-type counterpart? A crystallographic, biophysical, and theoretical study, hLife 2 (2024) 419–433, https://doi.org/10.1016/j.hlife.2024.06.003.

[12] Y.L. Ng, C.K. Salim, J.J.H. Chu, Drug repurposing for COVID-19: Approaches, challenges and promising candidates, Pharmacol. Ther. 228 (2021) 107930, https://doi.org/10.1016/j.pharmthera.2021.107930.

[13] J. Pardo, A.M. Shukla, G. Chamarthi, A. Gupte, The journey of remdesivir: From Ebola to COVID-19, Drugs, Context 9 (2020) 2020–4–14, https://doi.org/10.7573/dic.2020-4-14.

[14] G.R. Painter, M.G. Natchus, O. Cohen, W. Holman, W.P. Painter, Developing a direct acting, orally available antiviral agent in a pandemic: The evolution of molnupiravir as a potential treatment for COVID-19, Curr. Opin. Virol. 50 (2021) 17–22, https://doi.org/10.1016/j.coviro.2021.06.003.

[15] W.P. Painter, W. Holman, J.A. Bush, F. Almazedi, H. Malik, N.C.J.E. Eraut, M.J. Morin, L.J. Szewczyk, G.R. Painter, Human safety, tolerability, and pharmacokinetics of molnupiravir, a novel broad-spectrum oral antiviral agent with activity against SARS-CoV-2, Antimicrob. Agents Chemother. 65 (2021) e02428–20, https://doi.org/10.1128/AAC.02428-20.

[16] A. Zumla, J.F.W. Chan, E.I. Azhar, D.S.C. Hui, K.-Y. Yuen, Coronaviruses — drug discovery and therapeutic options, Nat. Rev. Drug Discov. 15 (2016) 327–347, https://doi.org/10.1038/nrd.2015.37.

[17] P. Forster, L. Forster, C. Renfrew, M. Forster, Phylogenetic network analysis of SARS-CoV-2 genomes, Proc. Natl. Acad. Sci. USA. 117 (2020) 9241–9243, https://doi.org/10.1073/pnas.2004999117.

[18] L. Zhang, D. Lin, X. Sun, U. Curth, C. Drosten, L. Sauerhering, S. Becker, K. Rox, R. Hilgenfeld, Crystal structure of SARS-CoV-2 main protease provides a basis for design of improved α-ketoamide inhibitors, Science 368 (2020) 409–412, https://doi.org/10.1126/science.abb3405.

[19] Z. Jin, X. Du, Y. Xu, Y. Deng, M. Liu, Y. Zhao, B. Zhang, X. Li, L. Zhang, C. Peng, Y. Duan, et al., Structure of Mpro from SARS-CoV-2 and discovery of its inhibitors, Nature 582 (2020) 289–293, https://doi.org/10.1038/s41586-020-2223-y.

[20] C. Ma, M.D. Sacco, B. Hurst, J.A. Townsend, Y. Hu, T. Szeto, X. Zhang, B. Tarbet, M.T. Marty, Y. Chen, Boceprevir, et al., GC-376, and calpain inhibitors II, XII inhibit SARS-CoV-2 viral replication by targeting the viral main protease, Cell Res. 30 (2020) 678–692, https://doi.org/10.1038/s41422-020-0356-z.

[21] S. Günther, P.Y.A. Reinke, Y. Fernández-García, J. Lieske, T.J. Lane, H.M. Ginn, F. H.M. Koua, C. Ehrt, W. Ewert, D. Oberthuer, et al., X-ray screening identifies active site and allosteric inhibitors of SARS-CoV-2 main protease, Science 372 (2021) 642–646, https://doi.org/10.1126/science.abf7945.

[22] E.C. Vatansever, K.S. Yang, A.K. Drelich, K.C. Kratch, C.C. Cho, K.R. Kempaiah, J. C. Hsu, D.M. Mellott, S. Xu, C.T.K. Tseng, et al., Bepridil is potent against SARS-CoV-2 *in vitro*, Proc. Natl. Acad. Sci. 118 (2021) e2012201118, https://doi.org/10.1073/pnas.2012201118.

[23] C. Ma, M.D. Sacco, Z. Xia, G. Lambrinidis, J.A. Townsend, Y. Hu, X. Meng, T. Szeto, M. Ba, X. Zhang, et al., Discovery of SARS-CoV-2 papain-like protease inhibitors through a combination of high-throughput screening and a FlipGFP-based reporter assay, ACS Cent. Sci. 7 (2021) 1245–1260, https://doi.org/10.1021/acscentsci.1c00519.

[24] H. Tan, Y. Hu, P. Jadhav, B. Tan, J. Wang, Progress and challenges in targeting the SARS-CoV-2 papain-like protease, J. Med. Chem. 65 (2022) 7561–7580, https://doi.org/10.1021/acs.jmedchem.2c00303.

[25] S. Yuan, X. Gao, K. Tang, J. Cai, M. Hu, P. Luo, L. Wen, Z. Ye, C. Luo, J.O.L. Tsang, et al., Targeting papain-like protease for broad-spectrum coronavirus inhibition, Protein Cell 13 (2022) 940–953, https://doi.org/10.1007/s13238-022-00909-3.

[26] Y. Zang, M. Su, Q. Wang, X. Cheng, W. Zhang, Y. Zhao, T. Chen, Y. Jiang, Q. Shen, J. Du, et al., High-throughput screening of SARS-CoV-2 main and papain-like protease inhibitors, Protein Cell 14 (2023) 17–27, https://doi.org/10.1093/procel/pwac016.

[27] B. Tan, X. Zhang, A. Ansari, P. Jadhav, H. Tan, K. Li, A. Chopra, A. Ford, X. Chi, F. X. Ruiz, et al., Design of a SARS-CoV-2 papain-like protease inhibitor with antiviral efficacy in a mouse model, Science 383 (2024) 1434–1440, https://doi.org/10.1126/science.adm9724.

[28] M. Bouhaddou, D. Memon, B. Meyer, K.M. White, V.V. Rezelj, M.C. Marrero, B.J. Polacco, J.E. Melnyk, S. Ulferts, R.M. Kaake, et al., The global phosphorylation landscape of SARS-CoV-2 infection, Cell 182 (2020) 685–712.e19, https://doi.org/10.1016/j.cell.2020.06.034.

[29] R. Wang, C.R. Simoneau, J. Kulsuptrakul, M. Bouhaddou, K.A. Travisano, J.M. Hayashi, J. Carlson-Stevermer, J.R. Zengel, C.M. Richards, P. Fozouni, et al., Genetic screens identify host factors for SARS-CoV-2 and common cold coronaviruses, Cell 184 (2021) 106–119 e14, https://doi.org/10.1016/j.cell.2020.12.004..

[30] T.H. Pham, Y. Qiu, J. Zeng, L. Xie, P. Zhang, A deep learning framework for high-throughput mechanism-driven phenotype compound screening and its application to COVID-19 drug repurposing, Nat. Mach. Intell. 3 (2021) 247–257, https://doi.org/10.1038/s42256-020-00285-9.

[31] L. Riva, S. Yuan, X. Yin, L. Martin-Sancho, N. Matsunaga, L. Pache, S. Burgstaller-Muehlbacher, P.D. De Jesus, P. Teriete, M.V. Hull, et al., Discovery of SARS-CoV-2 antiviral drugs through large-scale compound repurposing, Nature 586 (2020) 113–119, https://doi.org/10.1038/s41586-020-2577-1.

[32] X. Ju, Y. Zhu, Y. Wang, J. Li, J. Zhang, M. Gong, W. Ren, S. Li, J. Zhong, L. Zhang, et al., A novel cell culture system modeling the SARS-CoV-2 life cycle, PLoS Pathog. 17 (2021) e1009439, https://doi.org/10.1371/journal.ppat.1009439.

[33] Y. Yu, X. Ju, Q. Ding, A nucleocapsid-based transcomplementation cell culture system of SARS-CoV-2 to recapitulate the complete viral life cycle, Bio Protoc. 11 (2021) e4257, https://doi.org/10.21769/BioProtoc.4257.

[34] J.H. Zhang, T.D.Y. Chung, K.R. Oldenburg, A simple statistical parameter for use in evaluation and validation of high throughput screening assays, SLAS Discov. 4 (1999) 67–73, https://doi.org/10.1177/108705719900400206.

[35] L. Yang, L. Tian, L. Li, Q. Liu, X. Guo, Y. Zhou, R. Pei, X. Chen, Y. Wang, Efficient assembly of a large fragment of monkeypox virus genome as a qPCR template using dual-selection based transformation-associated recombination, Virol. Sin. 37 (2022) 341–347, https://doi.org/10.1016/j.virs.2022.02.009.

[36] Q. Peng, R. Peng, B. Yuan, J. Zhao, M. Wang, X. Wang, Q. Wang, Y. Sun, Z. Fan, J. Qi, et al., Structural and biochemical characterization of the nsp12-nsp7-nsp8 core polymerase complex from SARS-CoV-2, Cell Rep. 31 (2020) 107774, https://doi.org/10.1016/j.celrep.2020.107774.

[37] C. Subramani, G. Sharma, T. Chaira, T.K. Barman, High content screening strategies for large-scale compound libraries with a focus on high-containment viruses, Antiviral Res. 221 (2024) 105764, https://doi.org/10.1016/j.antiviral.2023.105764.

[38] H. Fan, L. Wang, W. Liu, X. An, Z. Liu, X. He, L. Song, Y. Tong, Repurposing of clinically approved drugs for treatment of coronavirus disease 2019 in a 2019-novel coronavirus-related coronavirus model, Chin. Med. J. (Engl.) 133 (2020) (2019) 1051–1056, https://doi.org/10.1097/CM9.0000000000000797.

[39] H. Ohashi, K. Watashi, W. Saso, K. Shionoya, S. Iwanami, T. Hirokawa, T. Shirai, S. Kanaya, Y. Ito, K.S. Kim, et al., Potential anti-COVID-19 agents, cepharanthine and nelfinavir, and their usage for combination treatment, iScience 24 (2021) 102367, https://doi.org/10.1016/j.isci.2021.102367.

[40] N. Drayman, J.K. DeMarco, K.A. Jones, S.-A. Azizi, H.M. Froggatt, K. Tan, N.I. Maltseva, S. Chen, V. Nicolaescu, S. Dvorkin, et al., Masitinib is a broad coronavirus 3CL inhibitor that blocks replication of SARS-CoV-2, Science 373 (2021) 931–936, https://doi.org/10.1126/science.abg5827.

[41] L. Shen, J. Zhao, Y. Xia, J. Lu, J. Sun, J. Tang, H. Xing, L. Yin, Y. Yang, C. Wang, Lycorine derivative effectively inhibits the replication of coronaviruses both

in vitro and *in vivo*, hLife 2 (2024) 75–87, https://doi.org/10.1016/j.hlife.2023.12.001.
[42] Y. Wen, S.L.F. Meyer, E.P. Masler, F. Zhang, J. Liao, X. Wei, D.J. Chitwood, Nematotoxicity of drupacine and a Cephalotaxus alkaloid preparation against the plant-parasitic nematodes Meloidogyne incognita and Bursaphelenchus xylophilus, Pest Manag. Sci. 69 (2013) 1026–1033, https://doi.org/10.1002/ps.3548.
[43] Y. Gao, L. Yan, Y. Huang, F. Liu, Y. Zhao, L. Cao, T. Wang, Q. Sun, Z. Ming, L. Zhang, et al., Structure of the RNA-dependent RNA polymerase from COVID-19 virus, Science 368 (2020) 779–782, https://doi.org/10.1126/science.abb7498.
[44] Y. Zhang, W. Song, S. Chen, Z. Yuan, Z. Yi, A bacterial artificial chromosome (BAC)-vectored noninfectious replicon of SARS-CoV-2, Antiviral Res. 185 (2021) 104974, https://doi.org/10.1016/j.antiviral.2020.104974.
[45] W. Vuong, M.B. Khan, C. Fischer, E. Arutyunova, T. Lamer, J. Shields, H.A. Saffran, R.T. McKay, M.J. van Belkum, M.A. Joyce, et al., Feline coronavirus drug inhibits the main protease of SARS-CoV-2 and blocks virus replication, Nat. Commun. 11 (2020) 4282, https://doi.org/10.1038/s41467-020-18096-2.
[46] L. Fu, F. Ye, Y. Feng, F. Yu, Q. Wang, Y. Wu, C. Zhao, H. Sun, B. Huang, P. Niu, et al., Both Boceprevir and GC376 efficaciously inhibit SARS-CoV-2 by targeting its main protease, Nat. Commun. 11 (2020) 4417, https://doi.org/10.1038/s41467-020-18233-x.
[47] L. Subissi, C.C. Posthuma, A. Collet, J.C. Zevenhoven-Dobbe, A.E. Gorbalenya, E. Decroly, E.J. Snijder, B. Canard, I. Imbert, One severe acute respiratory syndrome coronavirus protein complex integrates processive RNA polymerase and exonuclease activities, Proc. Natl. Acad. Sci. 111 (2014) E3900–E3909, https://doi.org/10.1073/pnas.1323705111.
[48] Q. Peng, R. Peng, B. Yuan, M. Wang, J. Zhao, L. Fu, J. Qi, Y. Shi, Structural basis of SARS-CoV-2 polymerase inhibition by favipiravir, The Innovation 2 (2021) 100080, https://doi.org/10.1016/j.xinn.2021.100080.
[49] J.J. Malin, I. Suárez, V. Priesner, G. Fätkenheuer, J. Rybniker, Remdesivir against COVID-19 and other viral diseases, Clin. Microbiol. Rev. 34 (2020) 00162-20, https://doi.org/10.1128/cmr.00162-20.
[50] L. Yan, Y. Huang, J. Ge, Z. Liu, P. Lu, B. Huang, S. Gao, J. Wang, L. Tan, S. Ye, et al., A mechanism for SARS-CoV-2 RNA capping and its inhibition by nucleotide analog inhibitors, Cell 185 (2022) 4347–4360.e17, https://doi.org/10.1016/j.cell.2022.09.037.
[51] Z. Jia, L. Yan, Z. Ren, L. Wu, J. Wang, J. Guo, L. Zheng, Z. Ming, L. Zhang, Z. Lou, et al., Delicate structural coordination of the severe acute respiratory syndrome coronavirus Nsp13 upon ATP hydrolysis, Nucleic Acids Res. 47 (2019) 6538–6550, https://doi.org/10.1093/nar/gkz409.
[52] D.D. Ho, Time to hit HIV, early and hard, N. Engl. J. Med. 333 (1995) 450–451, https://doi.org/10.1056/NEJM199508173330710.
[53] W. Sun, S. He, C. Martínez-Romero, J. Kouznetsova, G. Tawa, Xu. Miao, P. Shinn, E.G. Fisher, Y. Long, O. Motabar, et al., Synergistic drug combination effectively blocks Ebola virus infection, Antiviral Res. 137 (2017) 165–172, https://doi.org/10.1016/j.antiviral.2016.11.017.
[54] T. Bobrowski, L. Chen, R.T. Eastman, Z. Itkin, P. Shinn, C.Z. Chen, H. Guo, W. Zheng, S. Michael, A. Simeonov, et al., Synergistic and antagonistic drug combinations against SARS-CoV-2, Mol. Ther. 29 (2021) 873–885, https://doi.org/10.1016/j.ymthe.2020.12.016.
[55] Z.A. Shyr, Y.S. Cheng, D.C. Lo, W. Zheng, Drug combination therapy for emerging viral diseases, Drug Discov. Today 26 (2021) 2367–2376, https://doi.org/10.1016/j.drudis.2021.05.008.
[56] J. Chen, Q. Mu, X. Li, X. Yin, M. Yu, J. Jin, C. Li, Y. Zhou, J. Zhou, S. Suo, et al., Homoharringtonine targets Smad3 and TGF-β pathway to inhibit the proliferation of acute myeloid leukemia cells, Oncotarget 8 (2017) 40318–40326, https://doi.org/10.18632/oncotarget.16956.
[57] M. Qu, J. Li, L. Yuan, Uncovering the action mechanism of homoharringtonine against colorectal cancer by using network pharmacology and experimental evaluation, Bioengineered 12 (2021) 12940–12953, https://doi.org/10.1080/21655979.2021.2012626.
[58] H. Dong, Z. Wang, W. Meng, C. Li, Y. Hu, L. Zhou, X. Wang, The natural compound homoharringtonine presents broad antiviral activity *in vitro* and *in vivo*, Viruses 10 (2018) 601, https://doi.org/10.3390/v10110601.
[59] M. Hoffmann, H. Kleine-Weber, S. Schroeder, N. Krüger, T. Herrler, S. Erichsen, T. S. Schiergens, G. Herrler, N.-H. Wu, A. Nitsche, M.A. Müller, C. Drosten, S. Pöhlmann, SARS-CoV-2 cell entry depends on ACE2 and TMPRSS2 and is blocked by a clinically proven protease inhibitor, Cell 181 (2020) 271-280.e8, https://doi.org/10.1016/j.cell.2020.02.052.
[60] J.D. Gunst, N.B. Staerke, M.H. Pahus, L.H. Kristensen, J. Bodilsen, N. Lohse, L.S. Dalgaard, D. Brønnum, O. Fröbert, B. Hønge, et al., Efficacy of the TMPRSS2 inhibitor camostat mesilate in patients hospitalized with COVID-19-a double-blind randomized controlled trial, eClinicalMedicine 35 (2021) 100849, https://doi.org/10.1016/j.eclinm.2021.100849.
[61] E. Tobback, S. Degroote, S. Buysse, L. Delesie, L. Van Dooren, S. Vanherrewege, C. Barbezange, V. Hutse, M. Romano, I. Thomas, et al., Efficacy and safety of camostat mesylate in early COVID-19 disease in an ambulatory setting: a randomized placebo-controlled phase II trial, Int. J. Infect. Dis. 122 (2022) 628–635, https://doi.org/10.1016/j.ijid.2022.06.054.
[62] J. Liu, R. Cao, M. Xu, X. Wang, H. Zhang, H. Hu, Y. Li, Z. Hu, W. Zhong, M. Wang, Hydroxychloroquine, a less toxic derivative of chloroquine, is effective in inhibiting SARS-CoV-2 infection *in vitro*, Cell Discov. 6 (2020) 1–4, https://doi.org/10.1038/s41421-020-0156-0.
[63] M. Hoffmann, K. Mösbauer, H. Hofmann-Winkler, A. Kaul, H. Kleine-Weber, N. Krüger, N.C. Gassen, M.A. Müller, C. Drosten, S. Pöhlmann, Chloroquine does not inhibit infection of human lung cells with SARS-CoV-2, Nature 585 (2020) 588–590, https://doi.org/10.1038/s41586-020-2575-3.
[64] D.R. Boulware, M.F. Pullen, A.S. Bangdiwala, K.A. Pastick, S.M. Lofgren, E.C. Okafor, C.P. Skipper, A.A. Nascene, M.R. Nicol, M. Abassi, et al., A randomized trial of hydroxychloroquine as postexposure prophylaxis for Covid-19, N. Engl. J. Med. 383 (2020) 517–525, https://doi.org/10.1056/NEJMoa2016638.
[65] B.S. Abella, E.L. Jolkovsky, B.T. Biney, J.E. Uspal, M.C. Hyman, I. Frank, S.E. Hensley, S. Gill, D.T. Vogl, I. Maillard, et al., Prevention and Treatment of COVID-19 With Hydroxychloroquine (PATCH) Investigators, Efficacy and safety of hydroxychloroquine vs placebo for pre-exposure SARS-CoV-2 prophylaxis among health care workers: a randomized clinical trial, JAMA Intern. Med. 181 (2021) 195–202, https://doi.org/10.1001/jamainternmed.2020.6319.